Multifunctional Elastomer Nanocomposites with Functionalized Graphene Single Sheets

Bulent Ozbas,[1]* Christopher D. O'Neill,[1] Richard A. Register,[1] Ilhan A. Aksay,[1] Robert K. Prud'homme,[1] Douglas H. Adamson[2]

[1]Department of Chemical and Biological Engineering, Princeton University, Odian Street, Princeton, New Jersey 08544

[2]Department of Chemistry and Institute of Materials Science, Polymer Program, University of Connecticut, 97 North Eagleville Road, Storrs, Connecticut 06269

Correspondence to: R. K. Prud'homme (E-mail: prudhomm@princeton.edu) or D. H. Adamson (E-mail: adamson@uconn.edu)

Received 19 March 2012; accepted 20 March 2012; published online 9 April 2012
DOI: 10.1002/polb.23080

ABSTRACT: We demonstrate the use of functionalized graphene sheets (FGSs) as multifunctional nanofillers to improve mechanical properties, lower gas permeability, and impart electrical conductivity for several distinct elastomers. FGS consists mainly of single sheets of crumbled graphene containing oxygen functional groups and is produced by the thermal exfoliation of oxidized graphite (GO). The present investigation includes composites of FGS and three elastomers: natural rubber (NR), styrene–butadiene rubber, and polydimethylsiloxane (PDMS). All of these elastomers show similar and significant improvements in mechanical properties with FGS, indicating that the mechanism of property improvement is inherent to the FGS and not simply a function of chemical crosslinking. The decrease in gas permeability is attributed to the high aspect ratio of the FGS sheets. This creates a tortuous path mechanism of gas diffusion; fitting the permeability data to the Nielsen model yields an aspect ratio of ~1000 for the FGS. Electrical conductivity is demonstrated at FGS loadings as low as 0.08% in PDMS and reaches 0.3 S/m at 4 wt % loading in NR. This combination of functionalities imparted by FGS is shown to result from its high aspect ratio and carbon-based structure. © 2012 Wiley Periodicals, Inc. J Polym Sci Part B: Polym Phys 50: 910–916, 2012

KEYWORDS: elastomer; filler; graphene; multifunctional; nanocomposite

INTRODUCTION An objective of elastomer nanofiller research has been to simultaneously enhance or impart multiple properties such as mechanical strength, stiffness, electrical conductivity, and barrier properties.[1,2] Carbon nanotubes[3] (CNTs) and exfoliated nanoclays[4] (NCs) have generated interest as multifunctional nanofillers. Although CNTs enhance mechanical properties and can provide electrical conductivity, their needle-like structure prevents them from providing barrier properties. NCs provide mechanical reinforcement and barrier properties at low loadings; however, they impart no electrical conductivity to the matrix. Here, we introduce a multifunctional nanofiller for elastomers, functionalized graphene sheets (FGSs), that improves mechanical properties, imparts electrical conductivity, and enhances barrier properties.

We have previously described the production of FGS by the exfoliation of graphite to single sheets.[5,6] The process involves oxidation of graphite stacks to graphite oxide (GO), followed by rapid heating to partially reduce the GO with the evolution of gases that separate the stacks into predominantly single sheets. The final FGS powder, with a C:O atomic ratio of ~12:1, comprises flexible wrinkled sheets that by atomic force microscopy (AFM) measurements have an average thickness of 1.75 nm and lateral dimensions of ~100–1000 nm. The polar oxygen species on FGS provides a functional interface that enhances dispersion and interactions with polymer matrices. Although in the dry state FGS powder has a BET surface area between 300 and 700 m^2/g, measured by N_2 adsorption, for sonicated suspensions of FGS the surface area is determined as 1850 m^2/g, close to the theoretical limit of 2630 m^2/g. AFM measurements on solution-processed samples reveal that 80% of FGS is single sheets. The sp^2 carbon structure, shared by CNTs, suggests similar strengths and electrical conductivities for FGS and CNTs. The thin sheet geometry of FGS is similar to NCs and suggests a similar effect on barrier properties in elastomer nanocomposites. The strength, sheet geometry with high aspect ratio, flexibility, and electrical conductivity of FGS make it unique and suggest its use as a nanofiller for elastomers.[1,7] Additionally, as the sheets are exfoliated by a thermal rather than a solution technique, FGS does not contain the "oxidative debris" recently shown to be present in solvent-exfoliated GO materials.[8]

**Present address:* Air Products and Chemicals, Inc., Allentown, Pennsylvania 18195.

Additional Supporting Information may be found in the online version of this article.

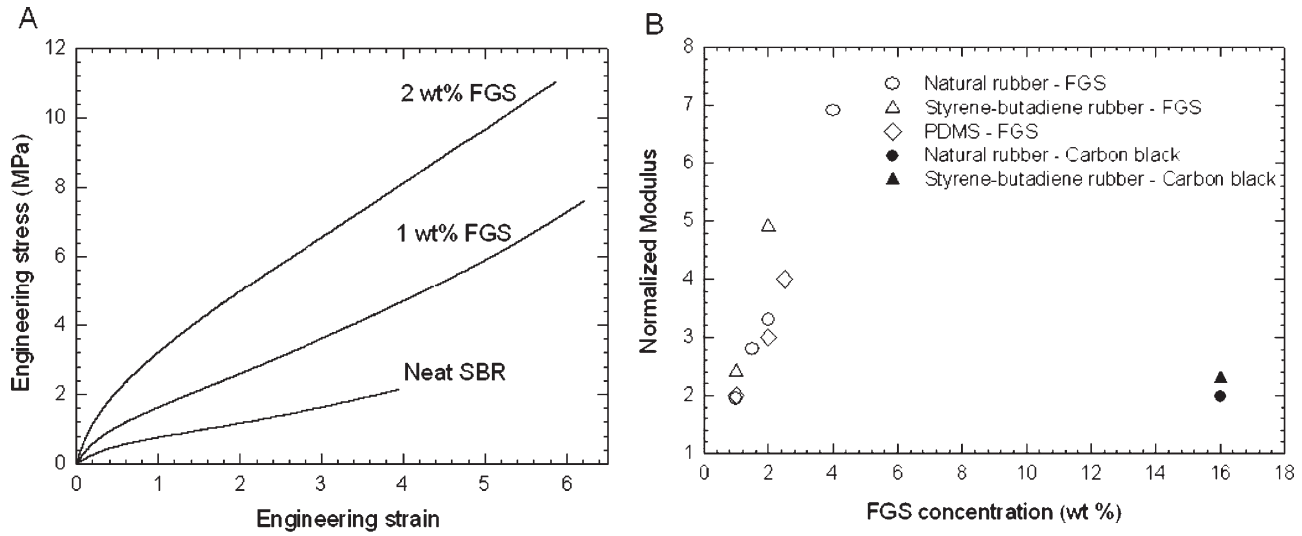

FIGURE 1 (A) Engineering stress–strain curves for neat SBR and 1 and 2 wt % FGS in SBR. (B) Normalized modulus values with respect to neat rubber for FGS-filled NR, SBR, and PDMS and CB-filled NR and SBR.

In this study, we present data on the mechanical, electrical, and barrier properties of FGS-filled elastomers. To show the generality of FGS as a nanofiller, several elastomers have been studied: natural rubber (NR), styrene–butadiene rubber (SBR), and polydimethylsiloxane (PDMS). The mechanical properties of FGS-filled NR and SBR are compared against the traditional carbon black (CB) filler. NR undergoes strain-induced crystallization, whereas SBR does not. Therefore, they represent two different classes of elastomers with different strengthening mechanisms. The electrical conductivities of FGS-filled NR and SBR are compared with literature values for CB and CNT fillers. Finally, the barrier properties of NR, SBR, and PDMS rubbers with FGS nanofillers are measured and compared against reported values for the same polymers filled with NCs. In each case, the FGS provides superior barrier performance. Therefore, the FGS nanofiller provides multifunctional enhancement of elastomer properties.

RESULTS AND DISCUSSION

Incorporation of FGS dramatically increases the modulus and tensile strength of the nanocomposites as shown in Figure 1(A), which compares neat and FGS-filled SBR. The engineering stress–strain curves exhibit moduli that increase by 150 and 400% with only 1 and 2 wt % FGS loading, respectively. Figure 1(B) shows that the same level of reinforcement is also seen in NR and PDMS elastomers, indicating the generality of the enhancement. Figure 1(B) also shows the much smaller relative increase in modulus for CB-filled samples. In CB-filled NR and SBR composites, 16 wt % loading is required to obtain the modulus enhancements achieved with only 1 wt % FGS. In addition, the levels of reinforcement achieved by FGSs are typically better than CNT[9–14] and clay-filled[15–23] elastomers as demonstrated in Figure 1(B). The values of modulus from 11 references are shown in the Supporting Information.

The modulus improvement in filled elastomers can arise from a combination of mechanisms. Micromechanical models such as Halpin–Tsai[24] and Mori–Tanaka[25] describe the modulus of a composite in terms of stiffness of the matrix and the filler stiffness, volume fraction, aspect ratio, shape, and orientation. In addition, stress transmission through direct particle contacts in aggregated network structures and changes in the crosslink density of the matrix may also play a role. Experiments were conducted to identify the key mechanisms operative in FGS-filled elastomers, although the interactions between mechanisms make an unambiguous assignment difficult. The modulus of the comparably rigid FGS or CB particles is expected to be several orders of magnitude larger than that of the soft rubbery matrix ($\sim$1 TPa vs. $\sim$1 MPa).[26] The Halpin–Tsai or Mori–Tanaka equations for the modulus of the composite predict that if the ratio of the modulus of a filler to that of the polymer matrix becomes larger than 100, further increase in filler modulus has a negligible effect on the composite modulus.[27] Therefore, for elastomers, the enhancement of mechanical properties by FGS over CB cannot be attributed to the high modulus of the filler alone.

Although filler modulus cannot explain the observed reinforcement ability, the geometry and aspect ratio of the FGS filler relative to CB do provide a reasonable explanation. The increase in modulus of the composite from FGS shown in Figure 1(B) can be compared with the predictions of the Halpin–Tsai equation,[23]

$$\frac{E}{E_2} = \frac{(E_1/E_2 + 1) + (L/H)((E_1/E_2) - 1)\varphi_1}{(E_1/E_2) + 1 - ((E_1/E_2) - 1)\varphi_1}, \qquad (1)$$

where E is the Young's modulus, φ the volume fraction, L/H is the aspect ratio of the filler with L being the length of the sheet and H the thickness, and the subscripts 1 and 2 refer to the filler and matrix, respectively. The relative ratio of the moduli of the filler and matrix is on the order of 10^6, the

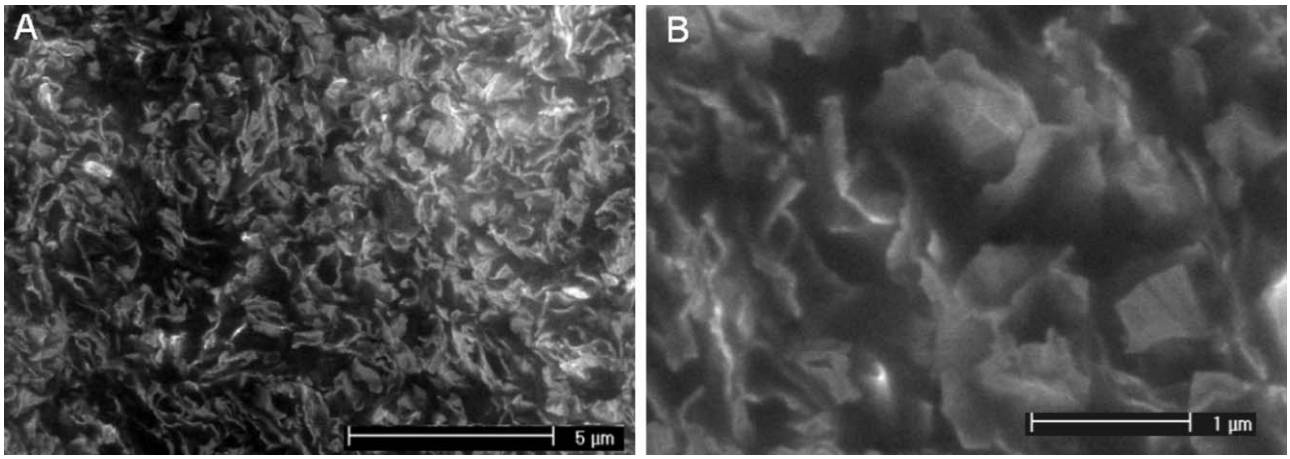

FIGURE 2 Scanning electron micrographs of uncoated, freeze-fractured 4 wt % FGS-NR nanocomposites at low (A) and high (B) magnifications.

density of FGS is taken as 2.0 g/cm^3, and the measured relative modulus of the composite at 1 vol % is $E/E_2 \sim 4$ as shown in Figure 1(B). From eq 1, this would predict an aspect ratio of the FGS sheets of ~300. This is to be compared to the value of 440 measured by AFM[5] for sheets that have been flattened on highly oriented pyrolytic graphite (HOPG) surfaces for measurement. The flexibility of the FGS sheets, which is visible in the scanning electron microscope (SEM) image of the freeze-fractured surface of the FGS-filled elastomer shown in Figure 2, would make the aspect ratio in the elastomer somewhat smaller than that observed by AFM.

An explanation of the reinforcement based solely on the nanofiller geometry presumes that the matrix is unaffected by the presence of FGS. According to the classical theory of rubber elasticity, the increase in modulus is an indication of an increase in crosslink density. The presence of functional groups on CB surfaces is believed to increase the number of crosslinks as chains are covalently and physically bonded to the CB.[28–30] The increase in modulus for FGS-filled elastomers may reflect this mechanism. As mentioned in the introduction, FGS contains oxygen functional groups. These functional groups, expected to be mainly epoxide and hydroxyls,[31] may incorporate into the crosslinking reactions and/or increase the adsorption of chains on the particle surface. Either covalent attachment or adsorption would lead to an increased modulus. Calorimetry measurements contained in the Supporting Information show that the rate of crosslinking is increased by the presence of FGS. However, the extent of crosslinking, as gauged by the heat evolved during the crosslinking reaction, appears to be similar in filled and unfilled NR. Therefore, we conclude that the 16-fold increase in modulus cannot be explained solely by differences in covalent crosslink formation.

If the increase in modulus was a result of additional effective crosslinks from strongly adsorbed chains on the surface of FGS,[32–36] then the effect should be sensitive to the chemical nature of the matrix polymer. Figure 1(B), however, shows that NR, SBR, and PDMS show nearly identical increases in modulus with filler concentration. Because the increase in stiffness with FGS loading shown in Figure 1 is relatively independent of matrix polymer type and because both bound polymer amounts and reaction chemistry would be expected to differ for the different matrices, we argue that any matrix effects are secondary relative to the effects of nanofiller geometry.

High-aspect-ratio materials, such as CNTs and FGS, enable both electrical and mechanical percolation at low volume fractions. Although percolation concentrations as low as 0.001 wt % have been reported for CNT-filled composites, other studies show concentrations as high as 2 wt % depending on the processing, alignment, chemistry of the CNTs, and matrix compatibility.[37–43] Electrical conductivity depends both on the number of contacts and the contact resistance, which are not known *a priori*. Figure 3(A) shows the change of conductivity as a function of filler concentration for two FGS samples (FGS-650 and FGS-400) of different surface area (650 and 400 m^2/g) in an uncured PDMS matrix. The differences in BET surface area values reflect different degrees of exfoliation. The conductivity of PDMS filled with FGS-650 shows electrical percolation at 0.8 wt %, whereas for FGS-400 as filler the transition is at 1.6 wt %. The differences in the extent of FGS exfoliation are also reflected in dynamic oscillatory rheological measurements, which are sensitive to stress transmission between particles and are a measure of interparticle contacts. The complex viscosity η^* increases sharply even before the FGS concentration exceeds the electrical percolation threshold, as shown in Figure 3(B). Dynamic oscillatory frequency sweeps [Fig. 3(C)] show that rheological percolation for FGS-650 occurs at 0.5 wt %. The frequency dependence of the storage and loss moduli, G' and G'', shows critical percolation at 0.5 wt % as demonstrated by the scaling[44–46] $G'(\omega) \sim G''(\omega) \sim \omega^1$. At a loading of 0.75 wt %, G' shows a broad, flat plateau indicating a strong network structure. Because mechanical stress transmission does not require direct particle contact, rheological measurements detect percolation at lower filler

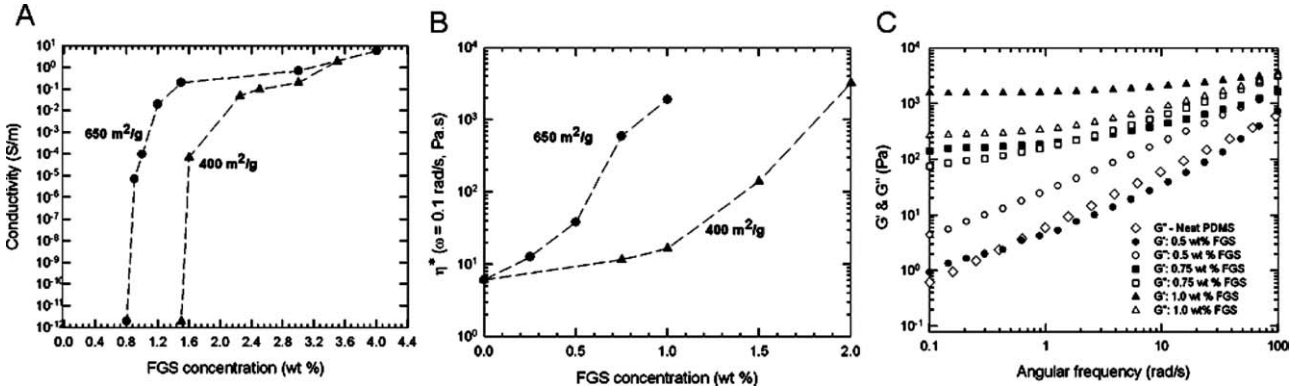

FIGURE 3 (A) Conductivity and (B) complex viscosity (η^*, measured at 0.1 rad/s angular frequency) of FGS-filled PDMS composites as a function of FGS concentration for FGS of two different BET surface areas (●: 650 m^2/g and ▲: 400 m^2/g). Dashed lines are guides to the eye. (C) Oscillatory frequency sweep tests (0.1% strain) for neat and FGS-filled PDMS base polymer. Closed symbols: storage modulus (G'). Open symbols: loss modulus (G'').

loadings than electrical conductivity, which requires more intimate particle-to-particle contact.

The SEM image of the 4 wt % FGS/NR freeze-fractured surface, shown previously in Figure 2, reveals well-dispersed FGS that does not restack into larger aggregated structures. This specimen was not coated with metal before SEM imaging; the fact that no significant charging or electron beam damage is observed during investigations at high magnifications and accelerating voltages (20 kV) reveals that the nanocomposite is electrically conductive. Using a four-point technique, the electrical conductivity of a 4 wt % FGS-NR nanocomposite was measured as 0.3 S/m. In contrast, in CB-filled systems, the polymer composites become conductive only at filler concentrations above 20 wt %.[47–49]

SEM images also reveal that individual sheets are not flat but rather have a wrinkled structure. Large-scale curvature arises from the intrinsic flexibility of the atomically thin sheets, whereas small-scale curvature arises from defects in the sp^2 structure induced by oxidation and partial reduction during exfoliation.[6,50] The wrinkled structure is crucial for the dispersion of FGS as it minimizes restacking of individual sheets. Flat structures with high aspect ratios have a tendency to restack from their exfoliated state because of the third power dependence of the attractive van der Waals' forces between flat sheets at close separation.[51] For example, it has been shown that suspended modified clay particles self-organize in various solvents into stacked structures with well-defined spacing.[52,53] Quantum mechanical calculations show that the effective dispersion attractions between FGS sheets are decreased fivefold because of the small-scale undulations found in GO sheets that keep separations to 0.76 nm rather than the 0.34-nm spacing in graphite.[5]

To investigate the effect of FGS filler on the gas permeability of elastomers, gas diffusion measurements through elastomer films with various loadings of FGS were conducted using a vacuum diffusion cell. Figure 4 shows the reduction of air permeability of PDMS nanocomposites as a function of FGS loading for two FGS samples. One FGS sample had a BET-measured surface area of 525 m^2/g and the other 320 m^2/g. With 1 and 5 wt % FGS (525 m^2/g), the permeability of PDMS is reduced by 50 and 80%, respectively. The reduction in permeability is sensitive to the nitrogen adsorption surface area of the FGS samples as surface area correlates with the degree of exfoliation of the graphene sheets. This can also be described in terms of the apparent aspect ratio of the FGS filler. In particle-filled systems, the permeability is mainly governed by tortuosity—the increased diffusion path length as penetrants diffuse laterally around the high-aspect-ratio impermeable particles. Such behavior is seen in clay-filled systems that show significant changes in permeability with different degrees of exfoliation.[54] The most widely used model to describe decreased permeability due to tortuosity is the 2D model of Nielsen.[55] The solid lines in Figure 4 show the predictions of the Nielsen model for the permeability of filled (P_F) and unfilled (P_U) films, written in terms of filler volume concentration (ϕ_F), length (L), thickness (H), and orientation factor (S):

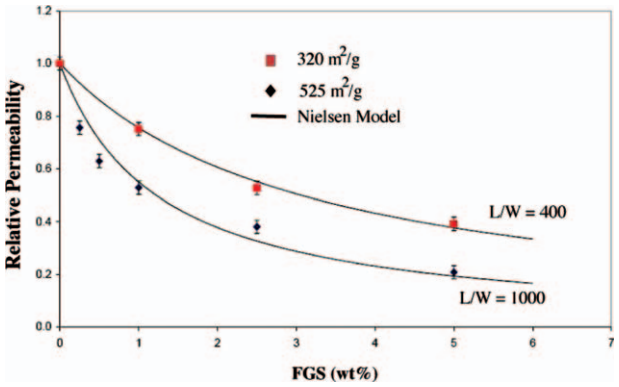

FIGURE 4 Effect of surface area (525 and 320 m^2/g) of FGS on the relative permeability of PDMS-FGS nanocomposites as a function of filler concentration. The solid lines represent the predictions of the Nielsen model for isotropically oriented sheets, where the key parameter of the impermeable filler is its length-to-height ratio (L/H).

$$\frac{P_F}{P_U} = \frac{1-\phi_F}{1+\frac{L}{2H}\phi_F\left(\frac{2}{3}\right)\left(S+\frac{1}{2}\right)}. \quad (2)$$

The L/H values are chosen as 1000 and 400, whereas S is set to zero, which corresponds to no orientation of filler particles in the polymer matrix. These values are again in reasonable agreement with the dimensions of the sheets measured by AFM.[5,54] The model predicts that even greater reductions in permeability could be achieved with alignment of the sheets perpendicular to the diffusion direction ($S = 1$): for $L/H = 1000$ and $S = 1$, the permeability would be reduced by more than one order of magnitude over the unfilled case at only 5 wt % FGS loading. The improvement in barrier properties for FGS-filled elastomers is greater than reported values for clay nanofillers in similar elastomer matrices (see Supporting Information for a detailed discussion).

CONCLUSIONS

FGS is shown to impart multifunctional performance to elastomeric matrices. Sixteen times higher loadings of traditional CB fillers are required to obtain the same stiffness as FGS. This reinforcement is observed equally for NR, SBR, and PDMS. FGS slightly accelerates the curing of NR, but the insensitivity of the increase in modulus to polymer type argues that the major mechanism of reinforcement does not arise from increased crosslink density but from the FGS nanofiller geometry. The mechanical reinforcement is consistent with composite models for oriented high-aspect-ratio fillers having aspect ratios of ~300. Loadings of 5 wt % FGS decrease the permeability to air by 80%. Fitting the permeability results to the Nielsen model for randomly oriented sheets gives an aspect ratio of ~1000, whereas direct AFM measurements on FGS sheets deposited on HOPG surfaces show aspect ratios of ~400. In addition to mechanical reinforcement and barrier properties, the FGS fillers impart electrical conductivity. The conductivity percolation threshold for FGS in PDMS is 0.8 wt %, and the conductivity of a 4 wt % FGS/NR nanocomposite is 0.3 S/m. Linear viscoelastic measurements show critical mechanical percolation at 0.5 wt % and a strong network structure by 0.75 wt %. Clearly, FGS imparts to elastomers a combination of properties unobtainable with CB, CNT, or clay nanofillers.

EXPERIMENTAL

Formation of FGSs

FGSs were produced by a two-stage process: oxidation of natural flake graphite to GO followed by exfoliation of GO into graphene sheets by rapid heating (2000 °C/min) to 1050 °C. X-ray diffraction showed that the resultant material does not exhibit peaks characteristic of graphite or GO. The details of this process and the characterization of the FGS are given elsewhere.[6] All NR and SBR formulations and compounded materials were provided by Lord Corporation (Erie, PA; see Supporting Information). For PDMS samples, two-component silicone elastomer kits were used with a 10:1 ratio of silicone liquid base to curing agent (see Supporting Information).

Preparation of Composites

All FGS-NR and FGS-SBR nanocomposites were prepared by solution processing. Rubber formulations (4 g) were completely dissolved in 100 mL of tetrahydrofuran (THF) with the aid of a magnetic stir bar. FGS was then added to the rubber solutions suspended in 10 mL of THF. After mixing the FGS-rubber-THF solution for an hour with a stir bar, THF was removed by evaporation at room temperature and pressure. Before vulcanization, the samples were left overnight in a vacuum oven at room temperature to remove residual THF. Control tensile test experiments were performed to demonstrate that the mechanical properties of unfilled formulated rubbers were not affected by solution processing. Samples of 16 wt % CB-NR were prepared using a Haake Mini-Lab twin screw extruder (Thermo Electron Corp.) using counter-rotating screws at 200 rpm for 30 min. The temperature of the extruder was kept at 90 °C or below to suppress vulcanization of the rubber during mixing. NR and SBR composites were pressed to 0.5-mm-thick films in a PHI melt press and vulcanized at 150 °C for 20 min or 160 °C for 30 min, respectively. To disperse FGS in PDMS, a putty knife was used to manually mix the FGS into the uncrosslinked PDMS on a glass plate. After mixing for 15 min, the curing agent was added with additional mixing for 5 min.

Instrumental Analysis

Tensile measurements were conducted on an Instron Model 1122 using a 50 kg load cell on ASTM D1708 dog-bone samples. The engineering strain rate was 2.28 min^{-1}. Young's moduli of the samples were calculated from the initial slope of engineering stress versus engineering strain curves. Conductivity was measured using a Keithley Model 6514 electrometer or a Keithley 2000 multimeter at room temperature by a four-probe technique. The conductivity of the sample (σ, S/m) was calculated using $\sigma = L/RA$, where L (m) is the distance between the copper electrodes attached to the surface of the polymer film, R is the measured resistance (Ω), and A (m^2) is the cross-sectional area.

The dispersion of FGS in NR was investigated using an FEI XL-30 field-emission SEM. The samples were freeze fractured below their glass transition temperature (~−60 °C) by cooling in liquid nitrogen. The samples were not coated before imaging. To measure the gas barrier properties of the FGS-filled polymer films, a diffusion cell was constructed. The cell consisted of a membrane holder (Millipore model XX4404700; Billerica, MA) that separated two chambers; one open to the atmosphere (upstream) and the other (downstream) initially under vacuum (~2 mTorr). The pressure change (dp/dt) in the downstream chamber was measured via a vacuum gauge (Varian model 531; Palo Alto, CA), and the air permeability (P) of the polymer nanocomposite was calculated from the linear response portion of the data (dp/dt =constant) using

$$P = \frac{dp}{dt}\left[\frac{V \times l \times 273}{p_1(A \times T)}\right] \times \left[\frac{1}{760}\right], \quad (3)$$

where V is the downstream volume, T the temperature (K), l the membrane thickness, A the membrane area, and p_1 is the upstream pressure (Torr).

Vulcanization Procedure

Vulcanization kinetics of filled and unfilled NR samples was measured by a differential scanning calorimeter (Perkin-Elmer DSC 7). First, the samples were equilibrated at 100 °C and then the temperature was rapidly (at the maximum heating rate) raised to 150 °C and held at that temperature. Rheological measurements on uncured PDMS dispersions were measured in a cone and plate geometry with a 25-mm-diameter 0.04 radian cone at ambient temperature on an Anton Paar MCR-501 rheometer.

ACKNOWLEDGMENTS

The authors acknowledge the support of the National Science Foundation MRSEC Program through the Princeton Center for Complex Materials award numbers DMR-0213706 and DMR-0819860. The authors also thank the Lord Corporation for their generous donation of rubber samples used in these investigations.

REFERENCES AND NOTES

1 Kim, H.; Abdala, A. A.; Macosko, C. W. *Macromolecules* **2010,** *43*, 6515–6530.

2 Kim, H.; Miura, Y.; Macosko, C. W. *Chem. Mater.* **2010,** *22*, 3441–3450.

3 Bokobza, L. *Polymer* **2007,** *48*, 4907–4920.

4 Sengupta, R.; Chakraborty, S.; Bandyopadhyay, S.; Dasgupta, S.; Mukhopadhyay, R.; Auddy, K.; Deuri, A. S. *Polym. Eng. Sci.* **2007,** *47*, 1956–1974.

5 McAllister, M. J.; Luen, J.-L.; Adamson, D. H.; Schniepp, H. C.; Abdala, A. A.; Lui, J.; Herrera-Alonso, M.; Milius, D. L.; Car, R.; Prud'homme, R. K.; Aksay, I. A. *Chem. Mater.* **2007,** *19*, 4396–4404.

6 Schniepp, H. C.; McAllister, M. J.; Sai, H.; Herrera-Alonso, M.; Adamson, D. H.; Prud'homme, R. K.; Car, R.; Saville, D. A.; Aksay, I. A. *J. Phys. Chem. B.* **2006,** *110*, 8535–8539.

7 Potts, J. R.; Dreyer, D. R.; Bielawski, C. W.; Ruoff, R. S. *Polymer* **2011,** *52*, 5–25.

8 Rourke, J. P.; Pandey, P. A.; Moore, J. J.; Bates, M.; Kinloch, I. A.; Young, R. J.; Wilson, N. R. *Angew. Chem. Int. Ed.* **2011,** *50*, 3173–3177.

9 Bokobza, L.; Kolodziej, M. *Polym. Int.* **2006,** *55*, 1090–1098.

10 Frogley, M. K.; Ravich, D.; Wagner, H. D. *Compos. Sci. Technol.* **2003,** *63*, 1647–1654.

11 Kim, Y. A.; Hayashi, T.; Endo, M.; Cotoh, Y.; Wada, N.; Seiyama, J. *Scr. Mater.* **2006,** *54*, 31–35.

12 Lopez-Manchado, M. A.; Biagiotti, J.; Valentini, L.; Kenny, J. M. *J. Appl. Polym. Sci.* **2004,** *92*, 3394–3400.

13 Fakhru'l-Razi, A.; Atieh, M. A.; Girun, N.; Chuah, T. G.; El-Sadig, M.; Biak, D. R. A. *Compos. Struct.* **2006,** *75*, 496–500.

14 Zhou, X. W.; Zhu, Y. F.; Liang, J. *Mater. Res. Bull.* **2007,** *42*, 456–464.

15 Vu, Y. T.; Mark, J. E.; Pham, L. H.; Engelhardt, M. *J. Appl. Polym. Sci.* **2001,** *82*, 1391–1403.

16 Wang, Y. Q.; Zhang, H. F.; Wu, Y. P.; Yang, J.; Zhang, L. Q. *J. Appl. Polym. Sci.* **2005,** *96*, 318–323.

17 Hwang, V. G.; Wei, K. *Polym. Eng. Sci.* **2004,** *44*, 2117–2124.

18 Joly, S.; Garnaud, G.; Ollitrault, R.; Bokobza, L.; Mark, J. E. *Chem. Mater.* **2002,** *14*, 4202–4208.

19 Lopez-Manchado, M. A.; Herrero, B.; Arroyo, M. *Polym. Int.* **2003,** *52*, 1070–1077.

20 Bala, P.; Samantaray, B. K.; Srivastava, S. K.; Nando, G. B. *J. Appl. Polym. Sci.* **2004,** *92*, 3583–3592.

21 Jia, Q. X.; Wu, Y. P.; Wang, Y. Q.; Lu, M.; Wang, J.; Zhang, L. Q. *J. Appl. Polym. Sci.* **2007,** *103*, 1826–1833.

22 Sadhu, S.; Bhowmick, A. K. *J. Polym. Sci. Part B: Polym. Phys.* **2004,** *42*, 1573–1585.

23 Wang, Y. Q.; Zhang, H. F.; Wu, Y. P.; Yang, J.; Zhang, L. Q. *J. Appl. Polym. Sci.* **2005,** *96*, 324–328.

24 Halpin, J. C.; Kardos, J. L. *Polym. Eng. Sci.* **1976,** *16*, 344–352.

25 Mori, T.; Tanaka, K. *Acta Metall. Mater.* **1973,** *21*, 571–574.

26 Edwards, D. C. *J. Mater. Sci.* **1990,** *25*, 4175–4185.

27 Sheng, N.; Boyce, M. C.; Parks, D. M.; Rutledge, G. C.; Abes, J. I.; Cohen, R. E. *Polymer* **2004,** *45*, 487–506.

28 Manna, A. K.; De, P. P.; Tripathy, D. K.; De, S. K.; Chatterjee, M. K. *Rubber Chem. Technol.* **1997,** *70*, 624–633.

29 Park, S. J.; Kim, J. S. *J. Colloid Interface Sci.* **2000,** *232*, 311–316.

30 Roychoudhury, A.; De, P. P. *J. Appl. Polym. Sci.* **1995,** *55*, 9–15.

31 Lerf, A.; He, H. Y.; Forster, M.; Klinowski, J. *J. Phys. Chem. B* **1998,** *102*, 4477–4482.

32 Berriot, J.; Montes, H.; Lequeux, F.; Long, D.; Sotta, P. *Macromolecules* **2002,** *35*, 9756–9762.

33 Litvinov, V. M.; Steeman, P. A. M. *Macromolecules* **1999,** *32*, 8476–8490.

34 Poompradub, S.; Tosaka, M.; Kohjiya, S.; Ikeda, Y.; Toki, S.; Sics, I.; Hsiao, B. S. *J. Appl. Phys.* **2005,** *97*, 103529.

35 Fukahori, Y. *Rubber Chem. Technol.* **2003,** *76*, 548–566.

36 Luo, H.; Kluppel, M.; Schneider, H. *Macromolecules* **2004,** *37*, 8000–8009.

37 Du, F. M.; Fischer, J. E.; Winey, K. I. *Phys. Rev. B* **2005,** *72*, 121404.

38 Sandler, J. K. W.; Kirk, J. E.; Kinloch, I. A.; Shaffer, M. S. P.; Windle, A. H. *Polymer* **2003,** *44*, 5893–5899.

39 Bryning, M. B.; Islam, M. F.; Kikkawa, J. M.; Yodh, A. G. *Adv. Mater.* **2005,** *17*, 1186–1191.

40 Sandler, J.; Shaffer, M. S. P.; Prasse, T.; Bauhofer, W.; Schulte, K.; Windle, A. H. *Polymer* **1999,** *40*, 5967–5971.

41 Ramasubramaniam, R.; Chen, J.; Liu, H. Y. *Appl. Phys. Lett.* **2003,** *83*, 2928–2930.

42 Du, F. M.; Scogna, R. C.; Zhou, W.; Brand, S.; Fischer, J. E.; Winey, K. I. *Macromolecules* **2004,** *37*, 9048–9055.

43 Du, F. M.; Fischer, J. E.; Winey, K. I. *J. Polym. Sci. Part B: Polym. Phys.* **2003,** *41*, 3333–3338.

44 Hess, W.; Vilgis, T. A.; Winter, H. H. *Macromolecules* **1998,** *21*, 2536–2542.

45 Schwittay, C.; Mours, M.; Winter, H. H. *Faraday Discuss.* **1995,** *101*, 93–104.

46 Winter, H. H.; Mours, M. In In Advances in Polymer Science, Vol. *134*; Ewen, B., Ed.; Springer, Berlin Heidelberg, New York, **1997;** pp 164–234.

47 Ishigure, Y.; Iijima, S.; Ito, H.; Ota, T.; Unuma, H.; Takahashi, M.; Hikichi, Y.; Suzuki, H. *J. Mater. Sci.* **1999,** *34*, 2979–2985.

48 Sau, K. P.; Chaki, T. K.; Kastgir, D. *J. Appl. Polym. Sci.* **1999,** *71*, 887–895.

49 Zhang, J.; Feng, S. J.; Wang, X. Q. *J. Appl. Polym. Sci.* **2004,** *94*, 587–592.

50 Li, J. L.; Kudin, K. N.; McAllister, M. J.; Prud'homme, R. K.; Aksay, I. A.; Car, R. *Phys. Rev. Lett.* **2006,** *96*, 176101.

51 Evans, D. F.; Wennerström, H. The Colloidal Domain, 2nd ed.; Wiley-VCH: New York, **1999**.

52 Connolly, J.; van Duijneveldt, J. S.; Klein, S.; Pizzey, C.; Richardson, R. M. *Langmuir* **2006,** *22*, 6531–6538.

53 Pizzey, C.; Klein, S.; Leach, E.; van Duijneveldt, J. S.; Richardson, R. M. *J. Phys.: Condens. Matter* **2004,** *16*, 2479–2495.

54 Xu, B.; Zheng, Q.; Song, Y. H.; Shangguam, Y. *Polymer* **2006,** *47*, 2904–2910.

55 Bharadwaj, R. K. *Macromolecules* **2001,** *34*, 9189–9129.